Research Article | Vol. 26, No. 23 | 12 Nov 2018 | OPTICS EXPRESS 31039
Optics EXPRESS

Time-resolved high-harmonic spectroscopy of ultrafast photoisomerization dynamics

KEISUKE KANESHIMA,* YUKI NINOTA, AND TARO SEKIKAWA

Division of Applied Physics, Hokkaido University, Sapporo, Hokkaido 060-8628, Japan
**kaneshima@eng.hokudai.ac.jp*

Abstract: We report the first time-resolved high-harmonic spectroscopy (TR-HHS) study of a chemical bond rearrangement. We investigate the transient change of the high-harmonic signal from 1,3-cyclohexadiene (CHD), which undergoes ring-opening and isomerizes to 1,3,5-hexatriene (HT) upon photoexcitation. We associated the harmonic yield variation with the changes in the molecule's electronic state and vibrational frequencies, which are caused by isomerization. This showed us that the electronic excited state of CHD created through two-photon absorption of 3.1 eV photons relaxes almost completely within 100 fs to the electronic ground state of CHD with vibrational excitation. Subsequently, the molecule isomerizes to HT (i.e., ring-opening occurs, around 400 fs after the excitation). The present results demonstrate that TR-HHS, which can track both electronic and nuclear dynamics, is a powerful tool for studying ultrafast photochemical reactions.

1. Introduction

1.1 Time-resolved high-harmonic spectroscopy

Measuring and understanding ultrafast dynamics in matter has always been a prime research objective. Recent developments related to ultrashort-pulse light sources have allowed the investigation of electronic dynamics at the attosecond and angstrom scales, and progress has been achieved by high-harmonic generation (HHG). HHG provides attosecond pulses in the extreme ultraviolet (EUV) and enables the development of time-resolved techniques at the attosecond scale [1–4].

HHG can be used not only as an ultrashort EUV light source but also as a tool to investigate the electronic state of the generating medium. The process of HHG can be explained as follows [5,6]: (i) A strong laser field tears a valence electron away from an atom or a molecule through tunnel ionization. (ii) The freed electron is accelerated by the laser electric field and then pulled back to its parent ion when the sign of the electric field reverses. (iii) The laser-driven electron recollides and recombines with its parent ion. As a result of recombination, the sum of the kinetic energy of the recolliding electron and its binding energy is released through coherent radiation (i.e., HHG). This radiation contains information about the electron-ion interaction. Hence, one can retrieve the electronic state of the generating medium from the amplitudes and phases of the high-harmonic spectra. This is known as high-harmonic spectroscopy (HHS) [7,8]. On account of the strong nonlinearity of the ionization process, the HHS of molecules can sensitively and selectively probe the highest occupied molecular orbitals (HOMOs), which are of prime importance for understanding chemical reactions.

HHS has been employed to study the ground-state electronic wavefunctions of gas-phase molecules [9–15]. In these studies, the technique of molecular alignment *via* rotational excitation [16] has been exploited to characterize the HHG from molecules as a function of their spatial orientations. Ultrafast molecular dynamics triggered by vibrational or electronic excitation have also been investigated via time-resolved HHS (TR-HHS), where the high-harmonic signals are monitored as a function of the pump-probe delay. TR-HHS has been used to investigate the vibrational dynamics of SF_6 [17] and N_2O_4 [18] and the

#341723 https://doi.org/10.1364/OE.26.031039
Journal © 2018 Received 7 Aug 2018; revised 30 Sep 2018; accepted 1 Oct 2018; published 9 Nov 2018

Optics EXPRESS

photodissociation dynamics of Br_2 [19], NO_2 [20], CH_3I, and CF_3I [21]. These experiments have shown that the HHG process is sensitive to both the valence electronic and the vibrational states of the molecules. Since chemical reactions result from the coupled dynamics of valence electrons and nuclei, the ability to simultaneously monitor the electronic and nuclear dynamics of molecules makes TR-HHS ideal for probing ultrafast chemical reactions.

However, the applications of TR-HHS were previously limited to photodissociation reactions of small molecules [19–21]. The TR-HHS of more complicated photoexcitation-induced reactions such as a concerted breakage and formation of bonds, i.e., a chemical bond rearrangement, remains a challenge. This limitation is mainly caused by the difficulty in observing high-harmonic signals from photoreactive organic molecules. Since these molecules are in a condensed phase at room temperature owing to their polarity and large molecular weights, their vapor pressure is not considered to be sufficiently high to observe high-harmonic signals [8].

In this study, we overcame this difficulty and demonstrated the TR-HHS of the ultrafast photoisomerization dynamics of 1,3-cyclohexadiene (CHD), C_6H_8. This is a significant advancement that makes TR-HHS a more versatile and practical tool for studying ultrafast chemical reactions.

1.2 Ultrafast photo-isomerization of 1,3-cyclohexadiene

CHD is a hydrocarbon ring molecule and exists in the liquid phase at room temperature. It undergoes ring-opening and isomerizes to 1,3,5-hexatriene (HT) upon photoexcitation [22,23] (Fig. 1). As a prototypical example of an electrocyclic reaction, this reaction is critical for understanding a large number of organic reactions, including the photo-induced formation of provitamin D [24,25]. It is being actively studied by novel ultrafast spectroscopic techniques such as x-ray fragmentation [26] and x-ray scattering [27] with femtosecond x-ray pulses that are obtained from a free-electron laser, photoelectron spectroscopy with single-order harmonic pulses [28,29], and near edge x-ray absorption fine structure at the carbon K-absorption edge with soft-x-ray high harmonics [30].

The ring-opening dynamics of CHD after excitation from the HOMO to the lowest unoccupied molecular orbital *via* one-photon absorption (1PA) is one of the most actively studied dynamics in time-resolved spectroscopy [26,27,29–40]. Most studies reported that the ring-opening step in the isomerization process is completed in less than 200 fs after photoexcitation. However, we observed that the ring opens at around 500 fs upon excitation from the HOMO to the $3p_x$-Rydberg state *via* two-photon absorption (2PA) using 3.1 eV photons, which is much slower than that observed in case of 1PA. In this experiment, we employed time-resolved photoelectron spectroscopy (TR-PES) using an isolated single-order harmonic at 29.5 eV [28] that was selected using a time-delay compensated monochromator [41–44]. Thus, another motivation of the present study is to confirm the delayed ring-opening of CHD upon 2PA by a spectroscopic method other than TR-PES; therefore, in this study, we employed TR-HHS. TR-PES and TR-HHS will provide complementary information because the former is sensitive to deep molecular orbitals, whereas the latter is sensitive to the shallowest orbital. Hence, we expected to obtain a deeper understanding of the ring-opening dynamics by comparing their results.

In addition, although CHD can adopt three distinct conformations after ring-opening, i.e., cZc-, tZt-, and cZt-HT (Fig. 1), the structural isomerization dynamics of the HTs after ring-opening have rarely been discussed in the femtosecond regime. In this study, we also endeavoured to clarify the structural-isomerization dynamics of the HTs using TR-HHS.

Optics EXPRESS

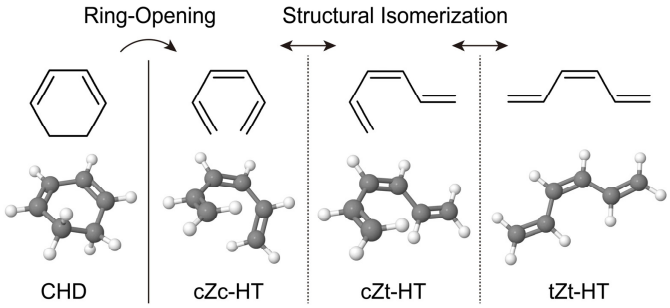

Fig. 1. Structural formulas and corresponding three-dimensional representations of CHD and its isomers.

2. Experimental methods

Figure 2 is a schematic diagram of our experiment. A beam from a 1-kHz-repetition-rate Ti:sapphire chirped-pulse amplifier passes through a 500-μm-thick LiB_3O_5 crystal for second-harmonic generation. Further, it is split into two color channels using a dichroic mirror. The delay, power, polarization, and dispersion of each channel were separately adjusted. The second harmonic (3.1 eV, 10 μJ, 74 fs full-width half-maximum (FWHM)) was used to excite an electron in CHD from the HOMO to the $3p_x$-Rydberg state [34,45–49] *via* 2PA (pump), whereas the fundamental (1.55 eV, 730 μJ, 30 fs FWHM) was used to generate high harmonics from CHD (probe). We recorded the high-harmonic yields as a function of the pump-probe delay. The separated beams were superimposed again using a dichroic mirror and collinearly focused using a concave mirror with a focal length of 500 mm. The intensities of the pump and probe pulses in the interaction region were estimated as 1.3 TW/cm^2 and 110 TW/cm^2, respectively. The relative polarizations of the pump and probe pulses were set to the magic angle (54.7°) to minimize the effect of impulsive alignment of CHD induced by the pump pulses. However, to the best of our knowledge, there exists no conclusive proof about the assumption that the magic angle configuration is effective for HHG from CHD. Note that the intensity of the pump pulse (1.3 TW/cm^2) is much lower than that of the pulses used for impulsive alignment (this value typically exceeds 10 TW/cm^2) [50]; hence, the effect of impulsive alignment is expected to be negligibly small.

Liquid CHD (Sigma Aldrich, 97%), which was stored in a stainless-steel reservoir at room temperature, flowed continuously through a 1-cm-long hollow glass fiber (inner diameter: 100 μm) into a vacuum chamber with 1.6 atm He gas. We avoided heating the sample to prevent thermal decomposition. The harmonics generated from CHD were spectrally separated using an EUV spectrometer and were imaged onto an EUV-sensitive charge-coupled device camera. Each data point was obtained for an integration time of 2 s, and 20 scans of data set were accumulated. Two 200-nm-thick aluminum filters were placed in front of the spectrometer to filter out the pump and probe light. We confirmed that harmonics from He were not observed upon introducing He alone into the system.

Optics EXPRESS

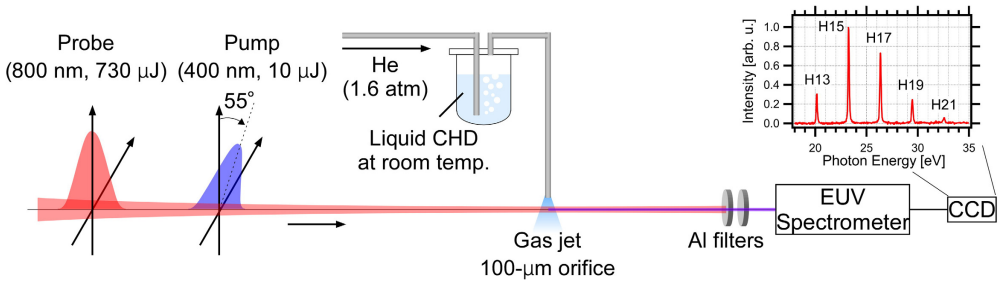

Fig. 2. Schematic of the experimental setup. Inset shows the observed harmonic spectrum.

3. Results

Figure 3 shows the experimentally observed harmonic yields from the CHD molecules, which were excited by 2PA of 3.1 eV photons, as a function of the pump-probe delay. Each harmonic yield was normalized to the average yield before pumping. The dips in the harmonic yields at zero delay are coherent artefacts arising from the overlap of the pump and probe. A polarization component orthogonal to the probe polarization was introduced by the pump, and it reduced the recombination probability in the HHG process. The full-width at half-minimum of the dips was ~80 fs, providing a high-order cross-correlation time between the pump and probe pulses. Fluctuations at the negative delays (shown in Fig. 3), except a small dip at around −100 fs, are due to instabilities in the experimental conditions; the dip at around −100 fs is due to the non-perfect Gaussian temporal intensity profile of the pump pulse. The pump-probe process with a role reversal, i.e., the process in which the intense probe pulse (800 nm) drives the CHD to an excited state and then the weak pump pulse (400 nm) stimulates XUV emission, does not cause the modulations at the negative delays. This is because the intensity of the pump pulse was only 1.3 TW/cm^2, which corresponds to a ponderomotive energy of 19 meV; this intensity is too low to generate high harmonics in the XUV.

After pumping, the yields of all observed harmonic orders displayed in Fig. 3 were modulated synchronously. These modulations are not merely fluctuations due to experimental instabilities because the modulation amplitudes after photoexcitation are sufficiently larger than those before photoexcitation. Then, what stimulates the intensity modulations of the high-harmonic signals? A previous study reported that the high-harmonic signals were modulated by the vibrational modes stimulated by impulsive stimulated Raman scattering (ISRS) via non-resonant excitation [17]. On the other hand, in the present case, the molecules were excited to a real state. Hence, the observed modulations should be attributable to the vibrational modes stimulated by the ultrafast internal conversion from the excited state whose equilibrium geometry is different from that of the ground state [51,52]. In the previous TR-PES measurement, the relaxation time of the $3p_x$-Rydberg state of CHD was 37 ± 13 fs upon 2PA [28]. This rapid relaxation via internal conversion coherently excites low-frequency vibrational modes whose periods are longer than the excited state life time [51]. Note that it is impossible to avoid vibrational excitation via ISRS when ultrashort pump pulses are employed, and ISRS in non-excited molecules may result in a vibrational background. However, the intensity of the pump pulse in this experiment was 1.3 TW/cm^2; this intensity is ~38 times less than that of the pump pulse used to excite vibrations in SF_6 via ISRS (~50 TW/cm^2) [17]. Hence, the effect of ISRS is expected to be negligibly small as compared to the effect of electronic excitation.

As discussed in [17], both the ionization and recombination steps in HHG contribute to the modulation of the high-harmonic signal. Modulation of the ionization rate induced by the molecular vibrations affects all harmonic orders; this explains the synchronization of the modulations of all orders as seen in Fig. 3. On the other hand, the recombination step results

Optics EXPRESS

in the harmonic-order dependence of the modulation amplitudes because the returning electrons of higher-order harmonics have shorter de Broglie wavelengths and more sensitive to small displacements of the atoms. This is why the largest modulation was observed in the 19th harmonic (Fig. 3). Further, in the present case, the de Broglie wavelengths (Table 1) are of the same order as the diagonal length of CHD (Fig. 4). Hence, small differences in harmonic order can affect the sensitivity. Since the largest changes were observed for the 19th harmonic, we have focused on this harmonic in the following discussion. For the results of the analysis of the other harmonic orders, please refer to Appendix.

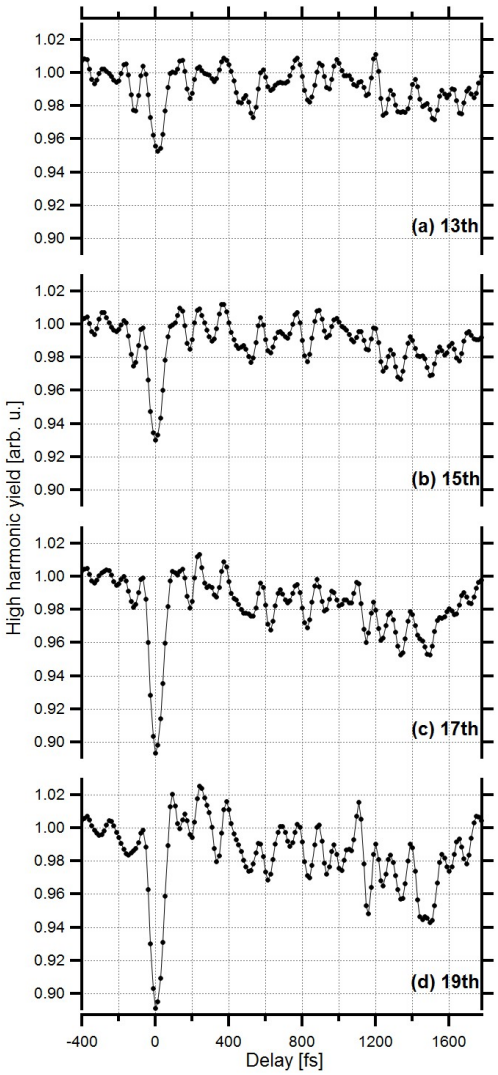

Fig. 3. Experimentally observed yields of the 13th to 19th harmonics as a function of the pump-probe delay.

Table 1. de Broglie wavelengths of the observed harmonics, assuming that the ionization energy of CHD is 8.25 eV [53].

	H13	H15	H17	H19
de Broglie wavelength [Å]	3.55	3.16	2.87	2.66

Optics EXPRESS

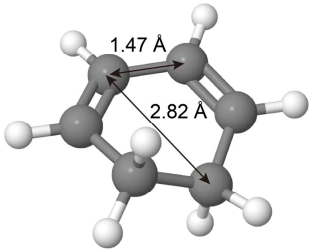

Fig. 4. Interatomic distances in CHD.

4. Discussion

4.1 Modulation frequency analysis

As the first step of analysis, we applied a short-time Fourier transform (STFT) with a 250 fs FWHM Gaussian window to the observed signal (Fig. 5) in order to extract the modulation frequencies. Before applying the STFT, we eliminated the DC component of the signal by high-pass filtering. As shown in Fig. 5(b), the spectrogram shows that the modulation frequencies changed at around 400 and 1000 fs. Further, by comparing Figs. 5(a) and 5(b), we also noticed that the harmonic yield itself also changed at around the same delays. The horizontal red lines in Fig. 5(a) depict the average values of the data points (black dots) within the range of length of each red line. The lines indicate the rough trend of the harmonic yield: the yield changed at around 400 and 1000 fs and was modulated with the characteristic frequencies around each average value. By considering that both the harmonic yield [Fig. 5(a)] and its modulation spectra [Fig. 5(b)] changed at around 400 and 1000 fs, we concluded that the molecule was isomerized at around these delays.

To observe more clearly the changes in the modulation frequency due to the isomerizations, we obtained colored curves (Fig. 6) by Fourier transforming the data points in the corresponding delay ranges, i.e., 80–400 fs [Fig. 6(a)], 400–1000 fs [Fig. 6(b)], and 1000–1600 fs [Fig. 6(c)]. The peak positions of the experimentally obtained spectra are indicated by black arrows. The figure clarifies the changes in molecular vibration upon isomerization.

4.2 Quantum chemistry calculations

Next, we tried to identify the isomers by associating the experimentally observed vibrational frequencies with the theoretically calculated vibrational modes of the isomers. Since vibrations are specific to a particular molecular structure, we can expect to identify the isomers. For this purpose, we performed quantum-chemical calculations of the ground states of CHD and its isomers at the LC-BLYP [54] /cc-pVDZ [55] level using GAMESS package [56,57]. The calculated vibrational modes of the isomers are listed in Table 2. The obtained results are well consistent with the results of previous studies on the experimental vibrational spectra of CHD [58] and tZt-HT [59]. Since cZc-HT and cZt-HT are unstable molecules, their static, i.e., non-transient, vibrational spectra can be obtained only via theoretical calculations.

Additionally, Table 3 lists the calculated HOMO energy levels of the isomers. For CHD and tZt-HT, the experimental values of the first ionization energies have been reported [53,60]. The calculated values are in agreement with the experimental values; thus, the accuracy of the calculations is validated. For cZc-HT and cZt-HT, no reference data were available. Note that it is difficult to simply associate the harmonic yield with the HOMO energy levels of the isomers. This is because it is necessary to consider the changes in the angular dependence of ionization probability and phase matching conditions, including the interference between the excited and the other unexcited molecules. Without accurate evaluation of these factors, the changes in the harmonic yield do not provide sufficient information to identify the isomers, though they indicate the occurrence of isomerization.

Optics EXPRESS

4.3 Dynamics of photo-excited 1,3-cyclohexadiene

In this section, we discuss the isomerization dynamics of CHD by comparing the experimentally obtained results with the quantum chemical calculation results. Table 2 presents a comparison of the theoretically calculated vibrational modes of CHD and the experimentally observed vibrational modes between 80 and 400 fs. In this delay range, we observed a vibrational mode at a frequency of 220 cm^{-1} [Fig. 6(a)]. This vibrational mode can be attributed to the ring-puckering mode (199 cm^{-1}) of CHD [58] (Table 2). Their correspondence indicates that the CHD photo-excited via 2PA of 3.1 eV photons remains unisomerized until around 400 fs. Further, the peak observed at 440 cm^{-1} in Fig. 6(a) is the second harmonic of the ring-puckering mode.

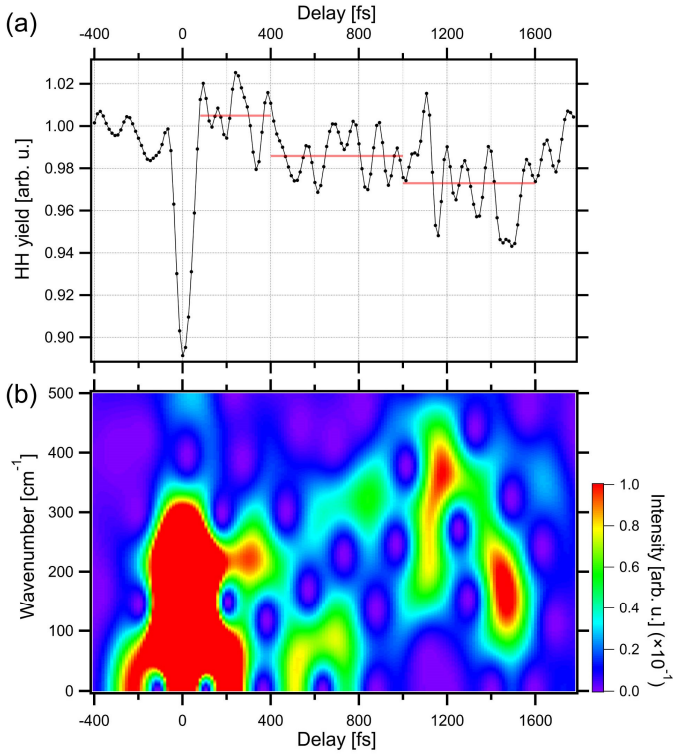

Fig. 5. (a) Experimentally observed yield of the 19th harmonic [identical to Fig. 3(d)]. The horizontal red lines show the average values of the data points (black dots) within the range of the length of each red line. (b) Short-time Fourier spectra of the transient harmonic yield [black dots in (a)].

Optics EXPRESS

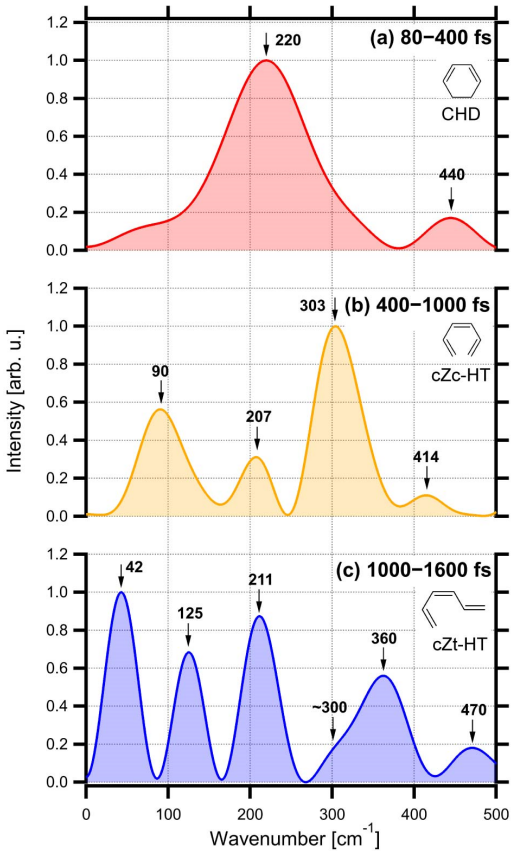

Fig. 6. Experimentally extracted modulation frequencies of the 19th harmonic yield (the colored curve in each panel). The curves were obtained by Fourier transforming the data points in the following delay ranges: (a) 80–400 fs, (b) 400–1000 fs, and (c) 1000–1600 fs. The black arrows depict the peak positions (in cm^{-1}) of the spectra.

However, it was unclear why the rest of the theoretically calculated vibrational mode of CHD listed in Table 2, i.e., the asymmetric vibrational modes at 302 and 469 cm^{-1}, were not observed in the experiment. We consider three possible explanations to clarify this point. The first one is that these vibrational modes are not excited in the present case. Since both the ground and excited electronic state ($3p_x$-Rydberg) of the CHD are symmetric [22], there is a possibility that only symmetric vibrational modes are induced by the internal conversion to the ground electronic state. In this case, asymmetric modes are neither induced nor observed. The second one is that the unobserved vibrational modes, though excited, scarcely modulate the harmonic yield. The third one is that these asymmetric vibrations are not observed at their fundamental frequencies. This mechanism is explained in the following paragraphs.

Consider a situation where there is a randomly oriented ensemble of a molecule, and the molecular vibrations are impulsively excited. In the case of the symmetric vibrational modes, the macroscopic responses of the ensemble at 1/4 and 3/4 period must be different from those at 0 and 1/2 period, i.e., the equilibrium state, as schematically shown in Fig. 7(a). Hence, the macroscopic high-harmonic signal generated from the ensemble is modulated by the symmetric vibrations. It is not clear whether the ensembles at 1/4 and 3/4 period enhance or suppress HHG. If one of them enhances and the other suppresses HHG, the harmonic yield is modulated at a vibrational frequency. Additionally, in this case, the second harmonic of the vibrational frequency will be observed if the magnitudes of the enhancement and the suppression are different. If both of the ensembles at 1/4 and 3/4 period enhance or suppress

Optics EXPRESS

HHG, the harmonic yield will be modulated at twice the vibrational frequency. In [17], all of the inversion symmetric modes of SF_6 were observed at their fundamental frequencies. In the present case, the lowest totally symmetric mode of CHD was also observed at the fundamental frequency (~199 cm^{-1}). These observations suggest that symmetric vibrational modes enhance and suppress HHG within their oscillation periods and are observed at their fundamental frequencies.

Table 2. Theoretically calculated and experimentally observed vibrational modes of CHD and its isomers.

Isomer and its point group	Frequency [cm^{-1}]			Symmetry
	Ab Initio (this work)	Experimental Refs. [a]	TR-HHS (this work)	
CHD (C_2)	199	198.7	220 and 440	A
	302	291		B
	469	467.6		B
cZc-HT (C_2)	91		90	A
	95			B
	165		207 and 414	A
	281			B
	303		303	A
cZt-HT (C_1)	103		125?	A
	153		125?	A
	201		211	A
	290		~300	A
	351		360	A
	467		470	A
tZt-HT (C_{2v})	101	102		B_2
	154	156		A_2
	170	170		A_1
	341	332		A_2
	346	354		B_1
	393	394		A_1

[a] [58] for CHD, and [59] for tZt-HT.

Table 3. Theoretically calculated HOMO energy levels (Calc.) and experimental values of the first ionization energies (Exp.) of CHD and its isomers.

	CHD	cZc-HT	tZt-HT	cZt-HT
Calc. (eV)	−8.27	−8.51	−8.28	−8.43
Exp. (eV)	8.25[a]	—	8.30[b]	—

[a] [53], [b] [60]

On the other hand, in the case of the asymmetric vibrational modes, the macroscopic responses of the ensemble at 1/4 and 3/4 period are identical [Fig. 7(b)]. Hence, the asymmetric modes modulate the harmonic yield at twice their vibrational frequencies. Therefore, the asymmetric vibrational modes were not observed at their fundamental frequencies.

The CHD, thus, remains in its vibrationally excited state until 400 fs. Furthermore, considering that the harmonic yields were observed to return to almost unity within ~80 fs [Figs. 3 and 5(a)], we can conclude that the electronic excited state of CHD almost completely relaxed to the ground state within 80 fs. If the CHD had stayed in the electronic excited state, the harmonic yield would have changed. In the previous TR-PES measurement, the relaxation time of the $3p_x$-Rydberg state of CHD was 37 ± 13 fs upon 2PA [28], which is consistent with the present result. Therefore, we conclude that the contribution of the excited state of CHD was obscured by the coherent artefact around the zero delay and that the CHD returned to its electronic ground state within 80 fs.

Since the absorbed photon energy of 6.2 eV is converted from electronic to vibrational energy via internal conversion, the molecule is located at an extremely high vibrational level of the electronic ground state. In other words, large amplitude vibrations are induced in the

Optics EXPRESS

molecule. Then, the excited vibrations drive the isomerization dynamics of CHD. Such vibrationally-driven isomerization after electronic relaxation was also observed in, e.g., rhodopsin [61,62]. In this case, furthermore, the coherent vibrations, especially in low-frequency modes whose periods are longer than the excited state lifetime, were observed even after the completion of the isomerization from rhodopsin to bathorhodopsin [51]. As discussed below, we also observed the coherent vibrations after the isomerization from CHD to HT. This indicates the isomerization completes faster than the periods of the observed vibrations.

The changes in the harmonic yield and the vibrational spectra at around 400 fs (Fig. 5) indicate the occurrence of isomerization at this moment. Table 2 presents a comparison of the theoretically calculated vibrational modes of cZc-HT with the experimentally observed vibrational frequencies between 400 and 1000 fs shown in Fig. 6(b). The observed peaks at 90 and 303 cm^{-1} are attributed to the symmetric vibrational modes of cZc-HT at 91 and 303 cm^{-1} in the theoretical calculation, respectively. Because of this consistency, we can conclude that CHD isomerizes to cZc-HT at around 400 fs. Further, the observed peak at 207 cm^{-1} can be attributed to the symmetric vibrational mode at 165 cm^{-1} in the theoretical calculation because of the appearance of its second harmonic at 414 cm^{-1}. On the other hand, the asymmetric mode at 95 cm^{-1} in the theoretical calculation, which should appear at 190 cm^{-1}, was missing in the present case.

Similarly, the changes in the harmonic yield and the vibrational spectra at around 1000 fs in Fig. 5 also indicate the occurrence of isomerization at this moment. Table 2 presents a comparison of the theoretically calculated vibrational modes of cZt-HT with the experimentally observed vibrational frequencies between 1000 and 1600 fs shown in Fig. 6(c). The observed peaks at 211, ~300, 360, and 470 cm^{-1} are attributed to the theoretically calculated modes at 201, 290, 351, and 467 cm^{-1}, respectively. Because of this consistency, we can conclude that cZc-HT isomerizes to cZt-HT at around 1000 fs. The observed peak at 125 cm^{-1} can be attributed to either of the theoretically calculated modes at 103 or 153 cm^{-1}. The peak observed at 42 cm^{-1} is attributed to the large molecular structure change during structural isomerization as none of the isomers have such a low frequency mode.

To summarize, the isomerization dynamics of the CHD after 2PA is as follows: (1) The excited CHD molecule relaxes to its ground state within 100 fs. (2) The vibrationally-driven isomerization from CHD to cZc-HT occurs at around 400 fs after the excitation. (3) Similarly, the vibrationally-driven isomerization from cZc-HT to cZt-HT occurs at around 1000 fs. (4) Thereafter, the molecule continues to isomerize using its vibrational energy.

Optics EXPRESS

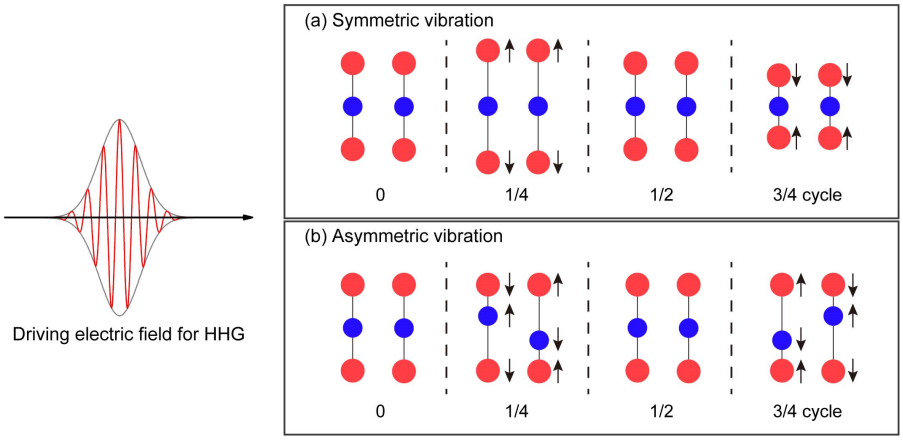

Fig. 7. Simplified schematic of the TR-HHS of the randomly oriented molecular ensemble with (a) symmetric vibration and (b) asymmetric vibration. The red and blue circles depict atoms, and the arrows depict atomic displacements.

4.4 Comparison with the results of time-resolved photoelectron spectroscopy

In our previous investigation using TR-PES, we also observed the ring-opening of CHD after 2PA at approximately 500 fs [28]. Here, we reconsider the results of the TR-PES experiment to verify its consistency with the aforementioned TR-HHS results. Figure 8 compares the results of TR-HHS and TR-PES. Figure 8(b) depicts the transient yields of photoelectrons obtained from the molecular orbitals (MOs) related to the C–C and CH_2 bonds (red) and from the MOs related to the C = C bonds (blue). Figure 8(c) depicts the difference between these photoelectron yields.

Comparison of the two results has provided us a more detailed understanding of the transient photoelectron yields of the TR-PES measurement: Since the increase in the difference in the photoelectron yield at around 400 fs [Fig. 8(c)] indicates a decrease in the number of C–C bonds and an increase in the number of C = C bonds, we ascribe this behavior to ring-opening [28]. Furthermore, the increase in this difference between 400 and 1000 fs can now be attributed to the atomic configuration evolution of cZc-HT, though we had previously considered it a sign of ring-opening from CHD to cZc-HT. At around 1000 fs, the photoelectron yields start to decrease [Fig. 8(b)], indicating that further isomerization occurs around this moment. In contrast, the difference remains almost constant after 1000 fs [Fig. 8(c)], indicating that the molecule remains in one of the hexatriene structures, which was identified as cZt-HT by the TR-HHS. The observed timescales and interpretations of TR-PES [28] and those of TR-HHS are thus entirely consistent with each other.

5. Summary

We have demonstrated the use of TR-HHS as a powerful tool for studying ultrafast photochemical reactions owing to its sensitivity to both electronic and nuclear dynamics. By associating the experimentally observed transient high-harmonic yields with the changes of the electronic states and vibrational spectra of the isomers, we elucidated the photoisomerization dynamics of CHD after 2PA by 3.1 eV photons. The excited CHD once relaxes to its ground electronic state, and vibrationally driven isomerization from CHD to cZc-HT, i.e., the ring-opening, occurs at around 400 fs after the excitation. Then, the vibrationally driven structural isomerization from cZc-HT to cZt-HT occurs at around 1000 fs. Further, the obtained results here provide detailed and complementary insights into the previously performed TR-PES study [28].

Optics EXPRESS

One final point must be made about the qualitative nature of our analysis approach. Herein, we compared the experimentally obtained modulation frequencies, which correspond to the frequencies of highly vibrationally excited molecules in the process of isomerization, with vibrational frequencies obtained from theoretical calculations of the ground state molecules. This intuitive approach offers only an approximate understanding of ultrafast isomerization dynamics. For complete understanding of the dynamics via TR-HHS, HHG simulation combined with quantum molecular dynamics simulation of photoexcited molecules will be necessary. Adopting this approach for complex molecules such as CHD is clearly a challenge to be tackled in the future.

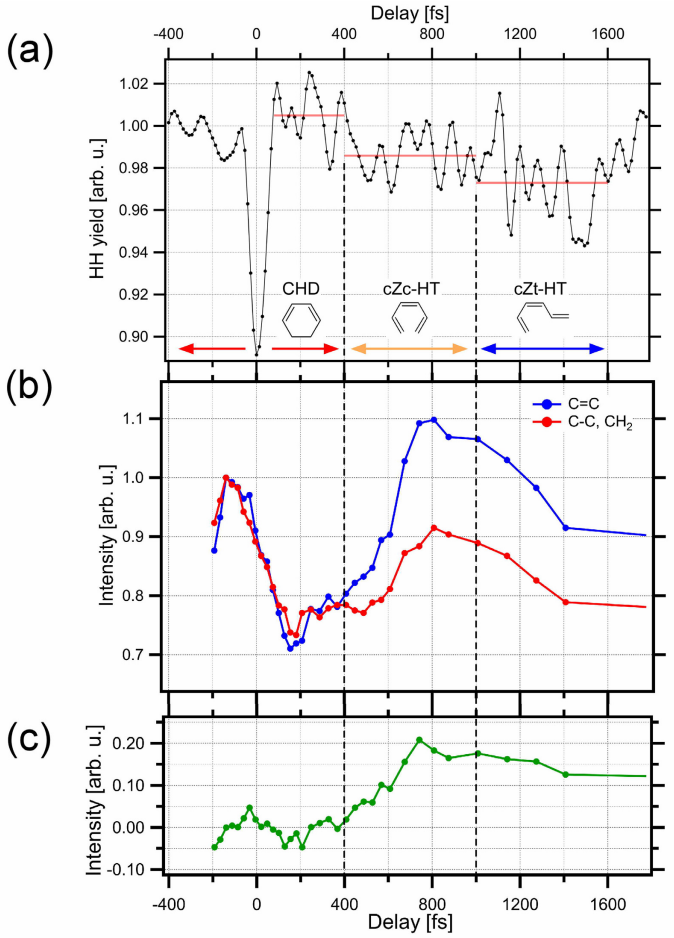

Fig. 8. (a) Results of TR-HHS [identical to Figs. 3(d) and 5(a)]. (b) Results of TR-PES [replot of Fig. 4(c) in [28]]. Red points indicate the time-dependent yield of photoelectrons mainly originating from the MOs related to the C–C and CH_2 bonds of CHD. Similarly, blue points show the yield of photoelectrons from the C = C bonds. (c) The result of subtracting the red points from the blue points in (b).

Funding

Core Research for Evolutional Science and Technology (CREST), JST (JPMJCR15N1); KAKENHI Japan Society for the Promotion of Science (15H03702 and 16K13854).

Optics EXPRESS

Appendix: Modulation frequency analysis of the observed harmonics

In this appendix, we present the results of the frequency analysis of all observed orders of harmonics (except for the 21st harmonic owing to its low signal-to-noise ratio). Different harmonic orders are sensitive to different spatial scales because of the different de Broglie wavelengths of their recombining electrons. Hence, these data are noteworthy because the differences between them may reflect the differences in their sensitivities to various spatial scales.

Figure 9 shows the results of the application of short-time Fourier transform (STFT) with a 250 fs FWHM Gaussian window to the observed harmonic signals. Before applying the STFT, we eliminated the DC components of the signals via high-pass filtering.

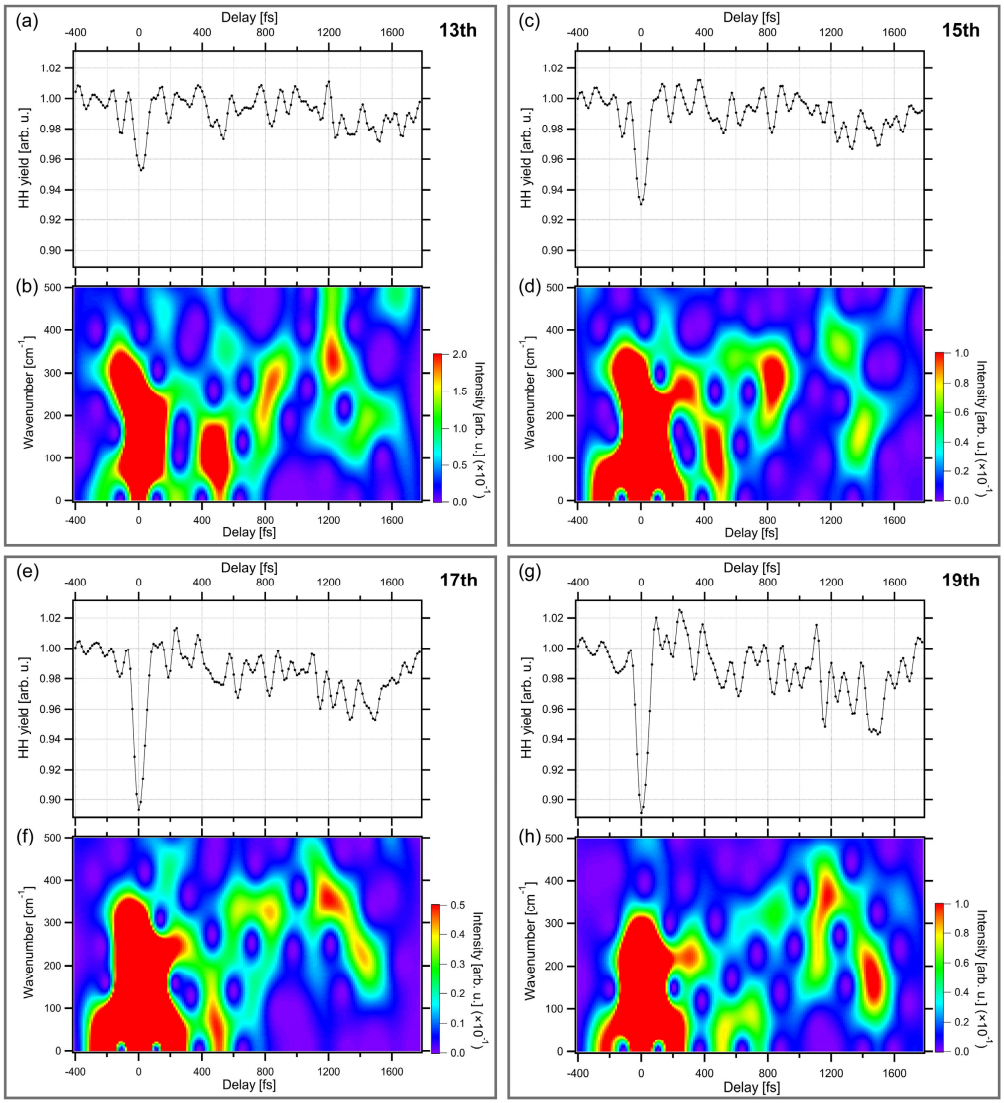

Fig. 9. (a) Experimentally observed yield of the 13th harmonic [identical to Fig. 3(a)]. (b) Short-time Fourier spectra of the transient harmonic yield [black dots in (a)]. The results for the other harmonic orders are similarly plotted.

To observe the changes in the modulation frequency more clearly, we obtained the power spectra (Fig. 10) by Fourier transforming the data points in the corresponding delay ranges of

Optics EXPRESS

Fig. 3, i.e., 80–400 fs (red curves), 400–1000 fs (yellow curves), and 1000–1600 fs (blue curves).

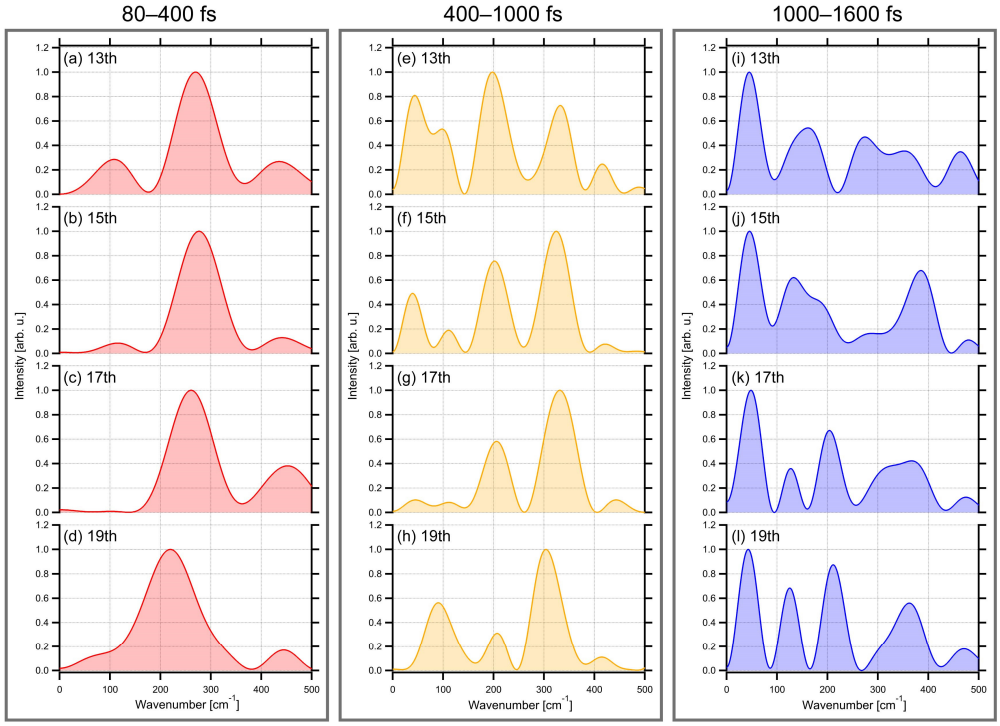

Fig. 10. Power spectra of the modulations observed in the delay range of 80–400 fs of each harmonic order (red curves). Each red curve was obtained by Fourier transforming the data points in the delay range of 80–400 fs of Fig. 3. Similarly, yellow and blue curves were obtained from the data points in the delay ranges of 400–1000 fs and 1000–1600 fs, respectively.

References and links

1. P. B. Corkum and F. Krausz, "Attosecond science," Nat. Phys. **3**(6), 381–387 (2007).
2. F. Krausz and M. Ivanov, "Attosecond physics," Rev. Mod. Phys. **81**(1), 163–234 (2009).
3. F. Krausz and M. I. Stockman, "Attosecond metrology: from electron capture to future signal processing," Nat. Photonics **8**(3), 205–213 (2014).
4. M. Nisoli, P. Decleva, F. Calegari, A. Palacios, and F. Martín, "Attosecond electron dynamics in molecules," Chem. Rev. **117**(16), 10760–10825 (2017).
5. K. J. Schafer, B. Yang, L. F. DiMauro, and K. C. Kulander, "Above threshold ionization beyond the high harmonic cutoff," Phys. Rev. Lett. **70**(11), 1599–1602 (1993).
6. P. B. Corkum, "Plasma perspective on strong field multiphoton ionization," Phys. Rev. Lett. **71**(13), 1994–1997 (1993).
7. S. Haessler, J. Caillat, and P. Salières, "Self-probing of molecules with high harmonic generation," J. Phys. At. Mol. Opt. Phys. **44**(20), 203001 (2011).
8. J. P. Marangos, "Development of high harmonic generation spectroscopy of organic molecules and biomolecules," J. Phys. At. Mol. Opt. Phys. **49**(13), 132001 (2016).
9. J. Itatani, J. Levesque, D. Zeidler, H. Niikura, H. Pépin, J. C. Kieffer, P. B. Corkum, and D. M. Villeneuve, "Tomographic imaging of molecular orbitals," Nature **432**(7019), 867–871 (2004).
10. T. Kanai, S. Minemoto, and H. Sakai, "Quantum interference during high-order harmonic generation from aligned molecules," Nature **435**(7041), 470–474 (2005).
11. X. Zhou, R. Lock, W. Li, N. Wagner, M. M. Murnane, and H. C. Kapteyn, "Molecular recollision interferometry in high harmonic generation," Phys. Rev. Lett. **100**(7), 073902 (2008).
12. S. Haessler, J. Caillat, W. Boutu, C. Giovanetti-Teixeira, T. Ruchon, T. Auguste, Z. Diveki, P. Breger, A. Maquet, B. Carré, R. Taïeb, and P. Salières, "Attosecond imaging of molecular electronic wavepackets," Nat. Phys. **6**(3), 200–206 (2010).

Optics EXPRESS

13. C. Vozzi, M. Negro, F. Calegari, G. Sansone, M. Nisoli, S. De Silvestri, and S. Stagira, "Generalized molecular orbital tomography," Nat. Phys. **7**(10), 822–826 (2011).
14. A. Rupenyan, J. B. Bertrand, D. M. Villeneuve, and H. J. Wörner, "All-optical measurement of high-harmonic amplitudes and phases in aligned molecules," Phys. Rev. Lett. **108**(3), 033903 (2012).
15. P. M. Kraus, A. Rupenyan, and H. J. Wörner, "High-harmonic spectroscopy of oriented OCS molecules: emission of even and odd harmonics," Phys. Rev. Lett. **109**(23), 233903 (2012).
16. H. Stapelfeldt and T. Seideman, "Colloquium : Aligning molecules with strong laser pulses," Rev. Mod. Phys. **75**(2), 543–557 (2003).
17. N. L. Wagner, A. Wüest, I. P. Christov, T. Popmintchev, X. Zhou, M. M. Murnane, and H. C. Kapteyn, "Monitoring molecular dynamics using coherent electrons from high harmonic generation," Proc. Natl. Acad. Sci. U.S.A. **103**(36), 13279–13285 (2006).
18. W. Li, X. Zhou, R. Lock, S. Patchkovskii, A. Stolow, H. C. Kapteyn, and M. M. Murnane, "Time-resolved dynamics in N_2O_4 probed using high harmonic generation," Science **322**(5905), 1207–1211 (2008).
19. H. J. Wörner, J. B. Bertrand, D. V. Kartashov, P. B. Corkum, and D. M. Villeneuve, "Following a chemical reaction using high-harmonic interferometry," Nature **466**(7306), 604–607 (2010).
20. H. J. Wörner, J. B. Bertrand, B. Fabre, J. Higuet, H. Ruf, A. Dubrouil, S. Patchkovskii, M. Spanner, Y. Mairesse, V. Blanchet, E. Mével, E. Constant, P. B. Corkum, and D. M. Villeneuve, "Conical intersection dynamics in NO_2 probed by homodyne high-harmonic spectroscopy," Science **334**(6053), 208–212 (2011).
21. A. Tehlar and H. J. Wörner, "Time-resolved high-harmonic spectroscopy of the photodissociation of CH_3I and CF_3I," Mol. Phys. **111**(14–15), 2057–2067 (2013).
22. S. Deb and P. M. Weber, "The ultrafast pathway of photon-induced electrocyclic ring-opening reactions: the case of 1,3-cyclohexadiene," Annu. Rev. Phys. Chem. **62**(1), 19–39 (2011).
23. B. C. Arruda and R. J. Sension, "Ultrafast polyene dynamics: the ring opening of 1,3-cyclohexadiene derivatives," Phys. Chem. Chem. Phys. **16**(10), 4439–4455 (2014).
24. M. Klessinger and J. Michl, *Excited States and Photochemistry of Organic Molecules* (VCH, 1995).
25. D. Feldman, J. W. Pike, and J. S. Adams, *Vitamin D* (Academic, 2011).
26. V. S. Petrović, M. Siano, J. L. White, N. Berrah, C. Bostedt, J. D. Bozek, D. Broege, M. Chalfin, R. N. Coffee, J. Cryan, L. Fang, J. P. Farrell, L. J. Frasinski, J. M. Glownia, M. Gühr, M. Hoener, D. M. P. Holland, J. Kim, J. P. Marangos, T. Martinez, B. K. McFarland, R. S. Minns, S. Miyabe, S. Schorb, R. J. Sension, L. S. Spector, R. Squibb, H. Tao, J. G. Underwood, and P. H. Bucksbaum, "Transient X-ray fragmentation: probing a prototypical photoinduced ring opening," Phys. Rev. Lett. **108**(25), 253006 (2012).
27. M. P. Minitti, J. M. Budarz, A. Kirrander, J. S. Robinson, D. Ratner, T. J. Lane, D. Zhu, J. M. Glownia, M. Kozina, H. T. Lemke, M. Sikorski, Y. Feng, S. Nelson, K. Saita, B. Stankus, T. Northey, J. B. Hastings, and P. M. Weber, "Imaging molecular motion: femtosecond x-ray scattering of an electrocyclic chemical reaction," Phys. Rev. Lett. **114**(25), 255501 (2015).
28. R. Iikubo, T. Sekikawa, Y. Harabuchi, and T. Taketsugu, "Structural dynamics of photochemical reactions probed by time-resolved photoelectron spectroscopy using high harmonic pulses," Faraday Discuss. **194**, 147–160 (2016).
29. S. Adachi, M. Sato, and T. Suzuki, "Direct observation of ground-state product formation in a 1,3-cyclohexadiene ring-opening reaction," J. Phys. Chem. Lett. **6**(3), 343–346 (2015).
30. A. R. Attar, A. Bhattacherjee, C. D. Pemmaraju, K. Schnorr, K. D. Closser, D. Prendergast, and S. R. Leone, "Femtosecond x-ray spectroscopy of an electrocyclic ring-opening reaction," Science **356**(6333), 54–59 (2017).
31. S. A. Trushin, W. Fuß, T. Schikarski, W. E. Schmid, and K. L. Kompa, "Femtosecond photochemical ring opening of 1,3-cyclohexadiene studied by time-resolved intense-field ionization," J. Chem. Phys. **106**(22), 9386–9389 (1997).
32. W. Fuß, W. E. Schmid, and S. A. Trushin, "Time-resolved dissociative intense-laser field ionization for probing dynamics: femtosecond photochemical ring opening of 1,3-cyclohexadiene," J. Chem. Phys. **112**(19), 8347–8362 (2000).
33. C.-Y. Ruan, V. A. Lobastov, R. Srinivasan, B. M. Goodson, H. Ihee, and A. H. Zewail, "Ultrafast diffraction and structural dynamics: the nature of complex molecules far from equilibrium," Proc. Natl. Acad. Sci. U.S.A. **98**(13), 7117–7122 (2001).
34. N. Kuthirummal, F. M. Rudakov, C. L. Evans, and P. M. Weber, "Spectroscopy and femtosecond dynamics of the ring opening reaction of 1,3-cyclohexadiene," J. Chem. Phys. **125**(13), 133307 (2006).
35. K. Kosma, S. A. Trushin, W. Fuss, and W. E. Schmid, "Cyclohexadiene ring opening observed with 13 fs resolution: coherent oscillations confirm the reaction path," Phys. Chem. Chem. Phys. **11**(1), 172–181 (2009).
36. M. Kotur, T. Weinacht, B. J. Pearson, and S. Matsika, "Closed-loop learning control of isomerization using shaped ultrafast laser pulses in the deep ultraviolet," J. Chem. Phys. **130**(13), 134311 (2009).
37. J. Kim, H. Tao, J. L. White, V. S. Petrović, T. J. Martinez, and P. H. Bucksbaum, "Control of 1,3-cyclohexadiene photoisomerization using light-induced conical intersections," J. Phys. Chem. A **116**(11), 2758–2763 (2012).
38. C. C. Pemberton, Y. Zhang, K. Saita, A. Kirrander, and P. M. Weber, "From the (1B) spectroscopic state to the photochemical product of the ultrafast ring-opening of 1,3-cyclohexadiene: a spectral observation of the complete reaction path," J. Phys. Chem. A **119**(33), 8832–8845 (2015).

Optics EXPRESS

39. O. Schalk, T. Geng, T. Thompson, N. Baluyot, R. D. Thomas, E. Tapavicza, and T. Hansson, "Cyclohexadiene revisited: a time-resolved photoelectron spectroscopy and ab Initio study," J. Phys. Chem. A **120**(15), 2320–2329 (2016).
40. S. L. Horton, Y. Liu, P. Chakraborty, S. Matsika, and T. Weinacht, "Vibrationally assisted below-threshold ionization," Phys. Rev. A (Coll. Park) **95**(6), 063413 (2017).
41. P. Villoresi, "Compensation of optical path lengths in extreme-ultraviolet and soft-x-ray monochromators for ultrafast pulses," Appl. Opt. **38**(28), 6040–6049 (1999).
42. L. Poletto, P. Villoresi, E. Benedetti, F. Ferrari, S. Stagira, G. Sansone, and M. Nisoli, "Intense femtosecond extreme ultraviolet pulses by using a time-delay-compensated monochromator," Opt. Lett. **32**(19), 2897–2899 (2007).
43. M. Ito, Y. Kataoka, T. Okamoto, M. Yamashita, and T. Sekikawa, "Spatiotemporal characterization of single-order high harmonic pulses from time-compensated toroidal-grating monochromator," Opt. Express **18**(6), 6071–6078 (2010).
44. H. Igarashi, A. Makida, M. Ito, and T. Sekikawa, "Pulse compression of phase-matched high harmonic pulses from a time-delay compensated monochromator," Opt. Express **20**(4), 3725–3732 (2012).
45. N. G. Minnaard and E. Havinga, "Some aspects of the electronic spectra of 1,3-cyclohexadiene, *(E)*- and *(Z)*-1,3,5-hexatriene," Recl. Trav. Chim. Pays Bas **92**(11), 1179–1188 (1973).
46. R. McDiarmid, A. Sabljic, and J. P. Doering, "Valence transitions in cis- and trans-hexatrienes," J. Am. Chem. Soc. **107**(4), 826–829 (1985).
47. M. Merchán, L. Serrano-Andrés, L. S. Slater, B. O. Roos, R. McDiarmid, and X. Xing, "Electronic spectra of 1,4-cyclohexadiene and 1,3-cyclohexadiene: a combined experimental and theoretical investigation," J. Phys. Chem. A **103**(28), 5468–5476 (1999).
48. W. Cheng, C. L. Evans, N. Kuthirummal, and P. M. Weber, "A 9 eV superexcited state of 1,3-cyclohexadiene revealed by double resonance ionization photoelectron spectroscopy," Chem. Phys. Lett. **349**(5–6), 405–410 (2001).
49. N. Kuthirummal and P. M. Weber, "Rydberg states: sensitive probes of molecular structure," Chem. Phys. Lett. **378**(5–6), 647–653 (2003).
50. F. Rosca-Pruna and M. J. J. Vrakking, "Revival structures in picosecond laser-induced alignment of I_2 molecules. I. Experimental results," J. Chem. Phys. **116**(15), 6567–6578 (2002).
51. C. Schnedermann, M. Liebel, and P. Kukura, "Mode-specificity of vibrationally coherent internal conversion in rhodopsin during the primary visual event," J. Am. Chem. Soc. **137**(8), 2886–2891 (2015).
52. R. Iikubo, T. Fujiwara, T. Sekikawa, Y. Harabuchi, S. Satoh, T. Taketsugu, and Y. Kayanuma, "Time-resolved photoelectron spectroscopy of dissociating 1,2-butadiene molecules by high harmonic pulses," J. Phys. Chem. Lett. **6**(13), 2463–2468 (2015).
53. K. Kimura, *Handbook of HeI Photoelectron Spectra of Fundamental Organic Molecules: Ionization Energies, Ab Initio Assignments, and Valence Electronic Structure for 200 Molecules* (Japan Scientific Societies, 1981).
54. H. Iikura, T. Tsuneda, T. Yanai, and K. Hirao, "A long-range correction scheme for generalized-gradient-approximation exchange functionals," J. Chem. Phys. **115**(8), 3540–3544 (2001).
55. T. H. Dunning, Jr., "Gaussian basis sets for use in correlated molecular calculations. I. The atoms boron through neon and hydrogen," J. Chem. Phys. **90**(2), 1007–1023 (1989).
56. M. W. Schmidt, K. K. Baldridge, J. A. Boatz, S. T. Elbert, M. S. Gordon, J. H. Jensen, S. Koseki, N. Matsunaga, K. A. Nguyen, S. Su, T. L. Windus, M. Dupuis, and J. A. Montgomery, "General atomic and molecular electronic structure system," J. Comput. Chem. **14**(11), 1347–1363 (1993).
57. M. S. Gordon and M. W. Schmidt, "Advances in electronic structure theory," in *Theory and Applications of Computational Chemistry* (Elsevier, 2005), pp. 1167–1189.
58. D. Autrey, J. Choo, and J. Laane, "Spectroscopic determination of the ring-twisting potential energy function of 1,3-cyclohexadiene and comparison with ab initio calculations," J. Phys. Chem. A **105**(45), 10230–10236 (2001).
59. N. C. Craig, M. C. Leyden, M. C. Moore, A. K. Patchen, T. Heuvel, T. A. Blake, T. Masiello, and R. L. Sams, "A reevaluation of the assignment of the vibrational fundamentals and the rotational analysis of bands in the high-resolution infrared spectra of trans- and cis-1,3,5-hexatriene," J. Mol. Spectrosc. **262**(1), 49–60 (2010).
60. M. Allan, J. Dannacher, and J. P. Maier, "Radiative and fragmentation decay of the cations of trans- and cis-1,3,5-hexatriene and of all trans-1,3,5-heptatriene in the $\tilde{A}(\pi^{-1})$ states, studied by emission and photoelectron–photoion coincidence spectroscopy," J. Chem. Phys. **73**(7), 3114–3122 (1980).
61. P. Kukura, D. W. McCamant, S. Yoon, D. B. Wandschneider, and R. A. Mathies, "Structural observation of the primary isomerization in vision with femtosecond-stimulated Raman," Science **310**(5750), 1006–1009 (2005).
62. P. J. M. Johnson, A. Halpin, T. Morizumi, V. I. Prokhorenko, O. P. Ernst, and R. J. D. Miller, "Local vibrational coherences drive the primary photochemistry of vision," Nat. Chem. **7**(12), 980–986 (2015).